

Stable knotted structure in spin-1 Bose-Einstein condensates with spin-orbit coupling

Yong-Kai Liu,^{1,*} Yun Liu,¹ and Shi-Jie Yang^{2,†}

¹*College of Physics and Information Engineering, Shanxi Normal University, Linfen 041004, China*

²*Department of Physics, Beijing Normal University, Beijing 100875, China*



(Received 15 November 2018; published 27 June 2019)

The recent experimental creation of knotted solitons in spin-1 Bose-Einstein condensates opens an interesting avenue for exploring the stability and dynamics of knot solitons. Knotted and helical vortices can be accommodated in spin-orbit-coupled antiferromagnetic spin-1 Bose-Einstein condensates. We demonstrate the stability of these topological structures via numerical simulations of the corresponding Gross-Pitaevskii equation. By changing the strength of the spin-orbit coupling, we find that the ground state undergoes a change from a knotted spin texture to a helical spin texture. Our results reveal that these types of topological object are experimentally realizable in spin-1 Bose-Einstein condensates.

DOI: [10.1103/PhysRevA.99.063626](https://doi.org/10.1103/PhysRevA.99.063626)

I. INTRODUCTION

Knotted and helical structures are intriguing topics in a variety of fields ranging from biophysics [1] and supramolecular chemistry [2,3] to many subfields in physics [4,5]. Recently, knots have been created experimentally in water [6], optical beams [7], and spinor Bose-Einstein condensates (BECs) [8], inspiring interest in the study of the stability and dynamics of knots.

Knots are topological solitons that are classified by the third homotopy group $\pi_3(S^2) \simeq Z$ [9–11], which establishes a mapping from a real space [three-dimensional (3D) sphere S^3] to a vector field S^2 and is classified by the Hopf charge Q . Unlike other topological excitations such as vortices, monopoles, and skyrmions which are classified by the winding numbers, knots can be interpreted as the linking number of preimages. The loops corresponding to the preimages cannot be unlinked by continuous deformations [12–14].

In the context of spin-1 BECs, the order parameter (OP) manifold of the polar phase is $M = S^2 \times U(1)/Z_2$ [9,10,15,16]. Here $U(1)$ is the manifold of the superfluid phase ϕ and S^2 is a two-dimensional sphere. The homotopy groups yield $\pi_n(M) \cong Z$ ($n = 1, 2, 3$). Previous experiments have created and observed two-dimensional skyrmions [17], an isolated monopole [18], and quantum knots in an antiferromagnetic spin-1 Bose-Einstein condensate using an external magnetic field [8]. There is a good correspondence between the experiment and the numerical simulation which theoretically describes the low-temperature dynamics of the condensate using the Gross-Pitaevskii equation with a time-dependent magnetic field.

The fact that skyrmions or knots can be created does not imply that they are energetically stable. It has been shown that the skyrmion and knot excitations are energetically unstable and will decay through expanding or shrinking in the antiferromagnetic spin-1 BEC [19]. Therefore, it is natural

to ask whether some additional stabilizing mechanisms can be adopted in searching for stable knots in spinor BECs. In the past few years, spin-orbit coupling (SOC) effects in two-component Bose-Einstein condensates have attracted a great deal of attention [20] due to the interplay between SOC and the unique properties of ultracold atoms. The recent experimental realization of SOC in the spin-1 BEC [21] opens an interesting avenue for exploring new quantum states and novel quantum phenomena in large-spin systems. Theoretical works have shown that the 2D skyrmions [22] can be naturally generated and stabilized by incorporating SOC into the spin-1 BEC. It is natural to ask if knots or other novel 3D spin textures are energetically stable in the spin-orbit-coupled antiferromagnetic spin-1 BECs.

In this paper we investigate the knotted and helical spin texture in the antiferromagnetic spin-1 Bose-Einstein condensates with SOC. By changing the strength of SOC, we demonstrate that they can be naturally generated from a vortex-free Gaussian wave packet. We display the phase diagram and the stable spin textures by numerically solving the coupled Gross-Pitaevskii equation. We try to use the concept of helical modulation to understand physically the emerged 3D structures. However, it is not exactly consistent with the numerical calculation because of the OP of the polar phase. It is also different from the two-component Bose-Einstein condensates with SOC, where the 3D skyrmion is perfectly explained by the helical modulation theory.

The paper is organized as follows. In Sec. II we present the mean-field theory of spin-1 BECs with SOC and the topological considerations of the knot in spin-1 BECs. In Sec. III we present numerical results of the BECs and describe the knot structure in comparison to the ideal knot in terms of particle density distributions and spin textures. A summary is given in Sec. IV.

II. THEORY

A. Hamiltonian

We consider a SOC $F = 1$ condensate system confined in a harmonic trap. The mean-field order parameter of the

*liuyongkai86@163.com

†yangshijie@tsinghua.org.cn

condensates can be described by a wave function $\psi(\mathbf{r}) = \sqrt{n(\mathbf{r})}\xi(\mathbf{r})$, where $n(\mathbf{r})$ is the local density and $\xi(\mathbf{r}) = (\xi_{+1}(\mathbf{r}), \xi_0(\mathbf{r}), \xi_{-1}(\mathbf{r}))^T$ is a normalized spinor [15,16]. The model Hamiltonian is given by $\mathcal{H} = \mathcal{H}_0 + \mathcal{H}_{\text{int}}$, with

$$\mathcal{H}_0 = \int d\mathbf{r} \Psi^\dagger \left[\frac{(\mathbf{k}^2 + 2\kappa\mathbf{k} \cdot \mathbf{A})}{2m} + V \right] \Psi \quad (1)$$

and

$$\mathcal{H}_{\text{int}} = \int d\mathbf{r} \left[\frac{c_0}{2} n^2 + \frac{c_2}{2} |\mathbf{F}|^2 \right], \quad (2)$$

where we employ the harmonic optical potential $V = m[\omega_\rho^2(x^2 + y^2) + \omega_z^2 z^2]/2$ and the non-Abelian gauge field \mathbf{A} . In addition, $\mathbf{F} = \sum_{m,n=-1}^1 \psi_m^*(\mathbf{r}) \hat{\mathbf{f}}_{mn} \psi_n(\mathbf{r})$ is the spin-polarization vector and the operators $\hat{\mathbf{f}}$ are the spin-1 matrices. The interaction term \mathcal{H}_{int} contains the spin-independent density-density interaction and the $|\mathbf{F}|$ -dependent interaction. The interaction strengths are given by the s -wave scattering length a_F in the spin- F channels of colliding spin-1 atoms as $c_0 = (g_0 + 2g_2)/3$ and $c_2 = (g_2 - g_0)/3$, with $g_F = 4\pi\hbar^2 a_F/M$. The system is ferromagnetic when the spin-spin interaction $c_2 < 0$ and polar when $c_2 > 0$.

B. Topological aspects

One can construct the general spinor wave function of the polar phase by applying a spin rotation and global condensate phase to the representative spinor $\zeta = (0, 1, 0)^T$ [9,23]. The general spinor in the polar phase is

$$\begin{aligned} \xi_p &= \hat{U}(\tau, \alpha, \beta) \begin{pmatrix} 0 \\ 1 \\ 0 \end{pmatrix} = \begin{pmatrix} e^{-i\alpha} \sin \beta \frac{(-1 + \cos \tau) \cos \beta - i \sin \tau}{\sqrt{2}} \\ \cos^2 \frac{\tau}{2} + \cos(2\beta) \sin^2 \frac{\tau}{2} \\ -e^{i\alpha} \sin \beta \frac{(-1 + \cos \tau) \cos \beta + i \sin \tau}{\sqrt{2}} \end{pmatrix} \\ &= \frac{1}{\sqrt{2}} \begin{pmatrix} -d_x + id_y \\ \sqrt{2}d_z \\ d_x + id_y \end{pmatrix}, \end{aligned} \quad (3)$$

where the matrix $\hat{U}(\tau, \alpha, \beta) = e^{-i\tau\mathbf{n}\cdot\mathbf{f}}$ and $\mathbf{n} = (\cos \alpha \sin \beta, \sin \alpha \sin \beta, \cos \beta)$. In the last identity the real-valued unit vector \mathbf{d} is referred to as the nematic vector. An ideal knot with linking number 1 is given by mapping \mathbf{n} as $S^3 \rightarrow S^2$. The radial profile function $\tau(r)$ meets the boundary conditions $\tau(0) = 2\pi$ and $\tau(\infty) = 0$ [10].

The nontrivial third homotopy group allows for the existence of knot which is characterized by the Hopf charge Q defined by [9]

$$Q_H = \frac{1}{4\pi^2} \int d^3\mathbf{r} \varepsilon_{ijk} \mathcal{F}_{ij} \mathcal{A}_k, \quad (4)$$

where $\mathcal{F}_{ij} = \partial_i \mathcal{A}_j - \partial_j \mathcal{A}_i = \mathbf{d} \cdot (\partial_i \mathbf{d} \times \partial_j \mathbf{d})$ is the strength of the gauge field and \mathcal{A}_k defines a connection in the order parameter space. For the knot, a point of \mathbf{d} corresponds to a closed curve in real space. A topological polar knot has linked preimages for every orientation of the nematic vector. The Hopf charge can be interpreted as the linking number of preimages, which provides an intuitive description [8].

III. NUMERICAL RESULTS

We first briefly review the 3D topological structures in two-component BECs with SOC [24,25]. A 3D skyrmion and 3D dimeron can be stabilized by incorporating the SOC into two-component BECs. The stability of the 3D skyrmion or 3D dimeron is physically understandable with the concept of helical modulation of the order parameter [24,26]. Under the simultaneous rotation of spin and real spaces $\text{SO}(3)_{R+S}$ in two-component BECs, the candidate state obtained theoretically by the helical spin modulation is verified to be the true ground state via numerical simulations. We try to apply this theory to a spin-1 BEC with the OP under the influence of a non-Abelian gauge field. The favorable OP can be written with the rotation matrix $\hat{V} = \exp(-i\varphi\mathbf{n} \cdot \mathbf{f})$ acting on the representative spinor, where $\mathbf{f} = (f_x, f_y, f_z)$ is the vector of the spin-1 matrices. The transformation rotates the spin around \mathbf{n} by an angle φ and the rotation axis \mathbf{n} corresponds to the modulation vector \mathbf{h} in the non-Abelian case [26]. The helical modulation of the OP for spin-1 BECs with SOC has been successfully applied to 2D skyrmion structures [22].

The problem on the 3D structure remains nontrivial because of the complexity of the order parameters in spin-1 BECs. In the following, we numerically minimize the full 3D Gross-Pitaevskii energy functional by using the imaginary-time-evolution scheme [27,28] with a spatial grid of $151 \times 151 \times 151$. For numerical calculations, we take $c_0 = 119$ and $c_2 = 3.7$, which correspond to the parameters of ^{23}Na and $\mathbf{A} = \kappa_\perp (f_x \hat{\mathbf{x}} + f_y \hat{\mathbf{y}}) + \kappa_z f_z \hat{\mathbf{z}}$. This is the 3D analog of the Rashba-type SOC as is known in the condensed matter context.

A. Knotted spin texture

If the Hamiltonian \mathcal{H} has $\text{SO}(3)_{R+S}$ symmetry in the polar phase as two-component BECs, an ideal knot will be created according to our theoretical analysis of the helical modulation for spin-1 BECs with SOC. In this case, The OP is written with the rotation matrix $\hat{V} = \exp(-i\varphi\mathbf{n} \cdot \mathbf{f})$. An appropriate $\varphi \sim \mathbf{k} \cdot \mathbf{r}$ to fulfill the OP manifold according to the wave function (3) will obtain an ideal knot texture.

However, the fact is that the helical modulation of the polar OP is not degenerate along all three directions [24]. An ideal knot cannot be created as in two-component BECs with SOC indicated by our numerical results. It is interesting to study what the 3D structure is in spin-1 BECs with SOC. As the theory of helical modulation works on the 2D skyrmion structures in spin-1 BECs with SOC [22], we focus on the broken structure in the z direction. We compare our numerical results with the ideal knot in the polar BEC. Here we take $\tau(r) = 2\pi[1 - \tanh(r/\xi_{\text{knot}})]$, with ξ_{knot} a characteristic size of the ideal knot.

Figure 1 shows the density profiles of $\psi_{\pm 1}$ and ψ_0 in the x - y plane. For the ideal knot, $\psi_{\pm 1}$ shows a double-ring pattern in the cross-sectional plane at $z = 0$, which fills the toroidal volume between the ψ_0 component. The ψ_0 component, which corresponds to d_z in Eq. (3), occupies the central region and the boundary, as well as the core around the central axis of the condensate. For the simulated results with SOC strength $\kappa = 2.3$, the density profiles of our numerical results coincide

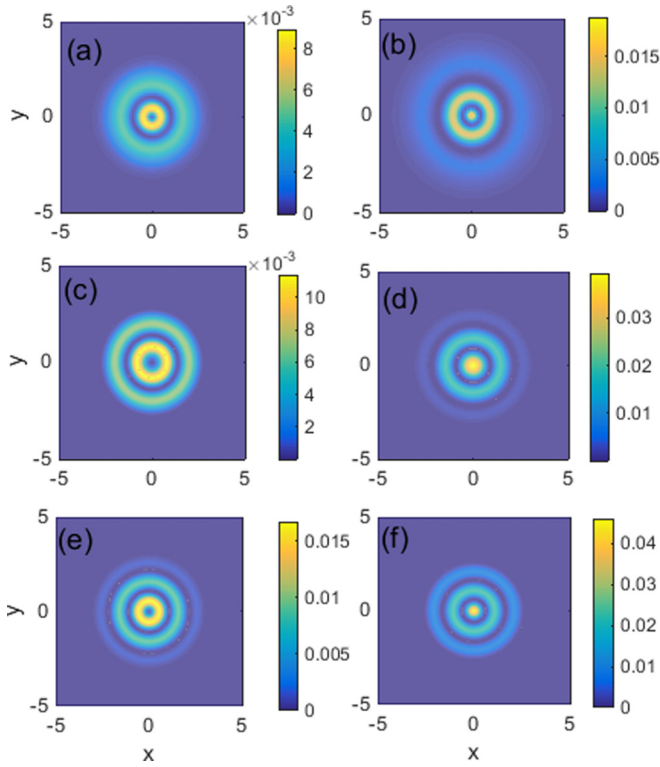


FIG. 1. Ideal and simulated density profiles of the spinor components in the x - y plane: density distributions of an ideal knot of (a) $\psi_{\pm 1}$ and (b) ψ_0 and density distributions of simulated results of (c) and (e) $\psi_{\pm 1}$ and (d) and (f) ψ_0 for SOC strength (c) and (d) $\kappa = 2.3$ and (e) and (f) $\kappa = 2.9$. All quantities in this figure and the following figures are dimensionless.

with the ideal knot. The region is a ring of depleted density of ψ_0 and enhanced density of the $\psi_{\pm 1}$ components. We have also checked that the phase distribution is the same between the theory and the simulation. With the continuous increase of the spin-orbit coupling strength κ , more density rings are generated as shown in Figs. 1(e) and 1(f).

Figure 2 shows the density profiles of $\psi_{\pm 1}$ and ψ_0 in the x - z plane. We note that the numerical results and the ideal knot are not exactly the same in the z direction, due to the fact that the polar OP is not degenerate along the entire 3D direction. The simulation results presented in Fig. 2 demonstrate that knotlike structure can be created with the appropriate parameter $\kappa = 2.3$, which looks like the ideal knot. From a topological point of view, the distribution of $\psi_{\pm 1}$ is the same in Figs. 2(a) and 2(c). There are differences for ψ_0 in Figs. 2(b) and 2(d), where surrounding the soliton core is the toroidal tube with a blemish of the loop boundary condition. This leads to an imperfect knotted structure at the boundary, which is caused by the breakage in the z direction. It does not happen in the two-component BECs with SOC. With the increase of SOC strength, the structure deviates away from the ideal knot. In Fig. 2(f) the two bilateral symmetry rings evolve into concentric rings, which means immediately that a spherical tube instead of a toroidal tube surrounds the soliton core. The interlinked structure is then corrupted because of changes in the internal core structure, which can be seen from the spin texture.

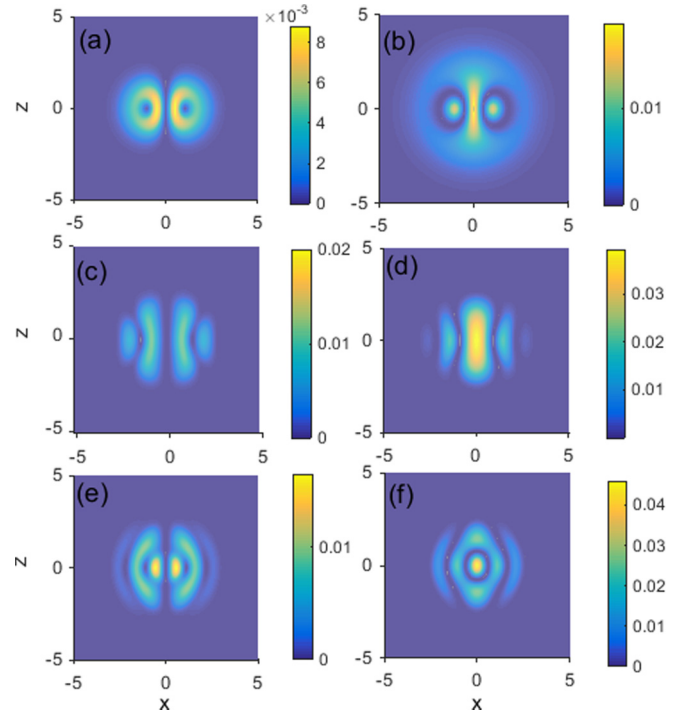


FIG. 2. Same as in Fig. 1 in the x - z plane.

In order to get a better view of our numerical results, we illustrate the preimages of the spin texture. Figure 3(a) shows the ideal knot in which the preimages of $\mathbf{d} = (\pm 0.98, 0, 0)$ and $\mathbf{d} = (0, 0, -0.98)$ are interlinked tubes. Here the tube describes a small isosurface around one point \mathbf{d} . Figure 3(b) is our simulated spin texture of the spin-1 condensates for $\kappa = 2.3$. It indeed reveals a structure similar to the ideal knot. We call it a knotlike structure, which preserves its knotted character. From Fig. 3(b) we see that the tubes are slightly broken, caused by the OP of the polar phase, but they do link with each other once. We also check other different points or areas on S^2 . The closer the points or areas are to $\mathbf{d} = (0, 0, 1)$, the more the tubes are broken. We can explain this by comparing Fig. 2(b) with Fig. 2(d). As ψ_0 corresponds to d_z in Eq. (3), $d_z = 1$ and the adjacent areas are ill-defined at the border. This only causes some tubes to be partially damaged and does not change the linking characteristics. If we repair the broken part, it will become the ideal knot. We have also calculated the Hopf charge defined by Eq. (4), which is approximately equal to 1 in the case of $\kappa = 2.3$. This indicates

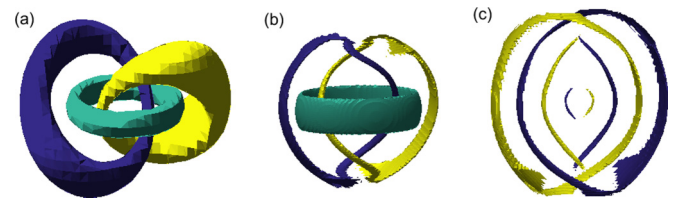


FIG. 3. Ideal and simulated preimages of the spin texture. (a) Preimage of $d_x = 0.98$ [yellow (light gray) tube], $d_x = -0.98$ [purple (dark gray) tube], and $d_z = -0.98$ [green (gray) tube] of an ideal knot. (b) Preimage of the simulated results for SOC strength $\kappa = 2.3$. (c) Same as in (b) but for $\kappa = 2.9$.

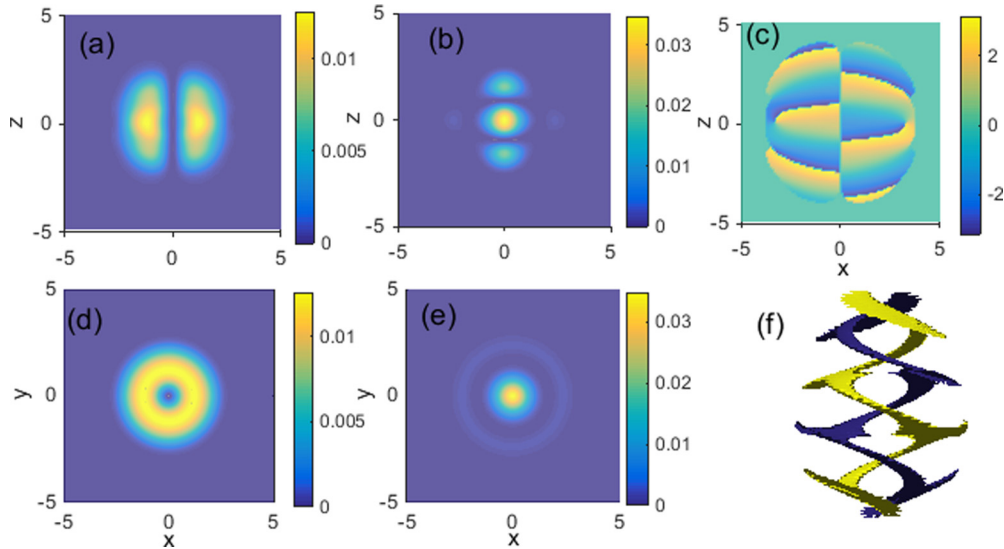


FIG. 4. Simulated images of the spinor components in the x - z plane for (a) $\psi_{\pm 1}$ and (b) ψ_0 . (c) Phase profile of the ψ_1 component. The density profiles in the x - y plane are for (d) $\psi_{\pm 1}$ and (e) ψ_0 . (f) Helical spin texture corresponding to $d_x = 0.98$ [yellow (light gray) tube] and $d_x = -0.98$ [purple (dark gray) tube] with $\kappa_{\perp} = 2.39$ and $\kappa_z = 2.69$.

that the broken area is not very large compared to the whole physical space and it is very similar to the ideal knot.

Based on our numerical results and analysis, we find that an ideal topological knot cannot be created or stabilized by incorporating SOC in the spin-1 BEC. However, we can get a stable knotlike structure which retains the linking character. The term knotlike means the absence of some boundary condition; thus, the Hopf number for the texture is not an integer and reflects the similarity with an ideal knot, while the linking character is preserved. The interlinking configuration decays as the strength of SOC increases further. In the meantime, new linking tubes are formed on the outside as in Fig. 3(c). This is 3D spin texture with linked and unlinked tubes in spinor BECs, which is different from two-component BECs with an increase of SOC. Although the theory of helical modulation is not completely applicable to the 3D structure in spin-1 BECs with SOC, it provides an intuitive picture. The emerged spin texture can be physically understandable with the helical modulation along the 3D radial direction, which is slightly broken in the z direction.

B. Helical spin texture

We now study the situation of $\kappa_{\perp} \neq \kappa_z$. We still obtain the knotted structures as κ_{\perp} slightly larger or smaller than κ_z . As κ_{\perp} is sufficiently larger than κ_z , it reduces to a 2D skyrmion. For $\kappa_{\perp} < \kappa_z$, a helical structure is generated [29,30]. The helical structures are analytically evaluated and shown in Fig. 4. Two semicircular areas are separated for $\psi_{\pm 1}$ in the x - z plane.

The density distributions are different from Fig. 1 in the x - y plane. Figure 4 shows that $|\psi_{\pm 1}|^2$ vanishes in the center and at infinity and the density is concentrated in a toroidal region. On the other hand, $|\psi_0|^2$ vanishes on a ring. It corresponds to a 2D skyrmion with unit topological charge, which is different from the knot in the x - y plane. The structure has helical preimages of d_x and d_y .

IV. SUMMARY

We have shown that SOC leads to the emergence of stable knotted and helical structures in antiferromagnetic spin-1 BECs. The influences of the strength and anisotropy of the SOC on the properties of the structures have also been investigated, which are different from two-component Bose-Einstein condensates with SOC. We find the knotted spin texture induced by the SOC is a knotlike texture, which is different from the ideal knot in spin-1 BECs. The emerged structures are physically understandable with the concept of the helical modulation and partially broken in the z direction. Our work provides an alternative way of creating knotlike structures and enriches the field of 3D spin-orbit coupling research in spinor BECs.

ACKNOWLEDGMENTS

This work was supported by the NSF of China under Grants No. 11604193 and No. 11774034 and the Natural Science Foundation for Young Scientists of Shanxi Province, China (Grant No. 201601D202012).

- [1] D. Meluzzi, D. E. Smith, and G. Arya, *Annu. Rev. Biophys.* **39**, 349 (2010).
 [2] D. Han, S. Pal, Y. Liu, and H. Yan, *Nat. Nanotechnol.* **5**, 712 (2010).

- [3] N. Ponnuswamy, F. B. Cougnon, J. M. Clough, G. D. Pantos, and J. K. Sanders, *Science* **338**, 783 (2012).
 [4] J. W. Cirtain, L. Golub, A. R. Winebarger, B. De Pontieu, K. Kobayashi, R. L. Moore, R. W. Walsh, K. E. Korreck,

- M. Weber, P. McCauley, A. Title, S. Kuzin, and C. E. DeForest, *Nature (London)* **493**, 501 (2013).
- [5] A. Vilenkin and E. P. S. Shellard, *Cosmic Strings and Other Topological Defects* (Cambridge University Press, Cambridge, 1994).
- [6] D. Kleckner and W. T. M. Irvine, *Nat. Phys.* **9**, 253 (2013).
- [7] M. R. Dennis, R. P. King, B. Jack, K. ÓHolleran, and M. J. Padgett, *Nat. Phys.* **6**, 118 (2010).
- [8] D. S. Han, M. W. Ray, K. Tiurev, E. Ruokokoski, A. H. Gheorghe, and M. Möttönen, *Nat. Phys.* **12**, 478 (2016).
- [9] Y. Kawaguchi and M. Ueda, *Phys. Rep.* **520**, 253 (2012).
- [10] Y. Kawaguchi, M. Nitta, and M. Ueda, *Phys. Rev. Lett.* **100**, 180403 (2008).
- [11] Y.-K. Liu, C. Zhang, and S.-J. Yang, *Phys. Lett. A* **377**, 3300 (2013).
- [12] T. Ollikainen, S. Masuda, M. Möttönen, and M. Nakahara, *Phys. Rev. A* **96**, 063609 (2017).
- [13] D.-L. Deng, S.-T. Wang, K. Sun, and L.-M. Duan, *Chin. Phys. Lett.* **35**, 013701 (2018).
- [14] W. Lee, A. H. Gheorghe, K. Tiurev, T. Ollikainen, M. Möttönen, and D. S. Hall, *Sci. Adv.* **4**, eaao3820 (2018).
- [15] T.-L. Ho, *Phys. Rev. Lett.* **81**, 742 (1998).
- [16] T. Ohmi and K. Machida, *J. Phys. Soc. Jpn.* **67**, 1822 (1998).
- [17] J.-Y. Choi, W. J. Kwon, and Y.-I. Shin, *Phys. Rev. Lett.* **108**, 035301 (2012).
- [18] M. W. Ray, E. Ruokokoski, K. Tiurev, M. Möttönen, and D. S. Hall, *Science* **348**, 544 (2015).
- [19] H. Zhai, W. Q. Chen, Z. Xu, and L. Chang, *Phys. Rev. A* **68**, 043602 (2003).
- [20] Y.-J. Lin, K. Jiménez-García, and I. B. Spielman, *Nature (London)* **471**, 83 (2011).
- [21] D. L. Campbell, R. M. Price, A. Putra, A. Valdés-Curiel, D. Trypogeorgos, and I. B. Spielman, *Nat. Commun.* **7**, 10897 (2016).
- [22] Y.-K. Liu and S.-J. Yang, *New J. Phys.* **19**, 063037 (2017).
- [23] H. Mäkelä, *J. Phys. A: Math. Gen.* **39**, 7423 (2006).
- [24] T. Kawakami, T. Mizushima, M. Nitta, and K. Machida, *Phys. Rev. Lett.* **109**, 015301 (2012).
- [25] Y.-K. Liu and S.-J. Yang, *Phys. Rev. A* **91**, 043616 (2015).
- [26] T. Kawakami, T. Mizushima, and K. Machida, *Phys. Rev. A* **84**, 011607(R) (2011).
- [27] W. Bao, D. Jaksch, and P. A. Markowich, *J. Comput. Phys.* **187**, 318 (2003).
- [28] W. Bao and H. Wang, *J. Comput. Phys.* **217**, 612 (2006).
- [29] M. Kobayashi and M. Nitta, *Nucl. Phys. B* **876**, 605 (2013).
- [30] Y.-K. Liu and S.-J. Yang, *Phys. Rev. A* **87**, 063632 (2013).